Polymer Testing 123 (2023) 108060

Contents lists available at ScienceDirect

Polymer Testing

journal homepage: www.elsevier.com/locate/polytest

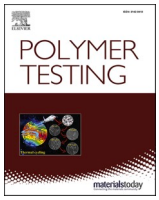

Assessing the shear viscous behavior of continuous carbon fiber reinforced PEKK composites with squeeze flow measurements

R. Arquier, G. Miquelard-Garnier, I. Iliopoulos, G. Régnier *

Laboratoire PIMM, Arts et Metiers Institute of Technology, CNRS, Cnam, HESAM Universite, 151 Boulevard de l'Hopital, Paris, 75013, France

ARTICLE INFO

Keywords:
Carbon fibers
Thermoplastic resin
Rheological properties
Consolidation

ABSTRACT

Out-of-autoclave processes of carbon fiber thermoplastic composites are gaining interest as they can drastically reduce the economic cost. To optimize consolidation, the flow behavior of these highly filled composites has to be characterized. Here, we propose to measure viscosity of carbon fiber/polyetherketoneketone through squeeze flow experiments in a rheometer. A modified Stefan's law assuming a power law fluid behavior with full anisotropy is developed for square and circular geometries to model the data. Values of the power law parameters K and n are obtained, on the order of 15,000 Pa.s^n and 0.02 at 1 bar. Though as expected independent of the samples' geometry and tapes' stacking, K and n depend on the applied pressure and plate size. This is due to localized shear which results in a shear-banding-like phenomenon. Finally, squeeze flow is compared to dynamic measurements and invalidate the Cox-Merz rule for such materials.

1. Introduction

Continuous carbon fibers (CF)/high performance thermoplastic composites are being developed especially for applications in the aerospace industry, due to their potential weldability as well as recyclability [1,2]. Recently among the polyaryletherketone (PAEK) family, polyetherketoneketone (PEKK)-based composites have gain interest over the more widely studied polyetheretherketone (PEEK) [3–5]. This is due to processing temperature that can be reduced while maintaining a high service temperature [6,7], as well as a tunable crystallinity [8,9].

Processing these composites consists in stacking several single plies (or tapes, which are typically 200 μm-thick with ≈ 55 %v of fibers), mostly using AFP (Automatic Fiber Placement). The stacks are then generally consolidated in an autoclave or press. This latter step aims at obtaining a low void content composite through the application of an appropriate pressure and temperature cycle. To reduce the energetic cost, out-of-autoclave (OOA) processes, such as VBO (Vacuum Bag Only) [10] or *in situ* consolidation during AFP [11–14]), are under development [15,16].

The main difficulty over thermosets composites is that high-performance thermoplastics display a high viscosity even at high temperature [2], for example ≈ 700 Pa s for PEKK (Kepstan® 7003) at 355 °C [17]. Due to the high content of continuous carbon fibers (CF), the global flow of the composite will be even more difficult. Hence, reducing the porosities in these thermoplastic composites to achieve the aerospace standards in terms of mechanical properties [18,19] is challenging, especially under low pressure and/or short consolidation times.

To understand and further optimize the consolidation, several authors have then tried to evaluate the rheology of such composites through oscillatory measurements. As the flow occurs almost only perpendicular to the fibers direction [20], the rheological test has to be adapted accordingly. Groves et al. [21,22] used off-centered square specimens to measure the viscosity of CF/PEEK composites. This, along with the use of analytical relations developed by Rogers [23], allowed to decouple the longitudinal and transverse components of the viscosity. More recently, Deignan et al. [24,25] updated this methodology by using rectangular specimens with a large aspect ratio to characterize the rheological behavior of CF/PEEK in the transverse direction only. The experiments were conducted on a single ply in order to avoid inter-ply slip [26], which is more pronounced for cross-ply composites [27]. Another strategy was proposed by Stanley et al. [28] who added a middle plate between the upper and the lower ones of a rheometer. This middle plate is then pulled out in a direction that remains perpendicular to the plies, thus also avoiding inter-ply slip. Either the axial or the transverse viscosity of CF/PEEK composites were then characterized by generating only intra-ply shear. Haanappel et al. [29] managed to measure the longitudinal shear viscosity of CF/PEEK composites by adapting a rheometer to set up a torsion bar test in which the fibers have

* Corresponding author.
E-mail address: gilles.regnier@ensam.eu (G. Régnier).

https://doi.org/10.1016/j.polymertesting.2023.108060
Received 9 May 2023; Accepted 11 May 2023
Available online 12 May 2023

the same direction as the torsion axis, avoiding again inter-ply slip. These measurements are all relatively complex but observe shear-thinning at all measured frequencies and hence describe a power law behavior for the composites, *i.e.* a viscosity having the following form (Eq. (1))

$$\eta = K\dot{\gamma}^{n-1} \quad (1)$$

where η is the viscosity, K and n are the parameters of the power law and $\dot{\gamma}$ the shear rate.

However, the values of the viscosity parameters obtained by these authors differ quite importantly from each other. Stanley et al. [28] obtained $K = 6700$ Pa.s^n and $n = 0.22$ for CF/PEEK (Solvay APC-2) at 380 °C. From Deignan's results [24] also on CF/PEEK (Suprem™ T60) at the same temperature, values ranging between 37,000 and 250,000 Pa. s^n can be extracted for K depending on the pressure applied (0.5 bar and 3 bar respectively), with n in the 0–0.1 range. Moreover, the direct correspondence between dynamic and steady-state measurements assuming the validity of Cox-Merz rule is still subject to debate for highly filled composites [29–31]. Hence the measurement of the composite viscosity in a shear flow may be more suitable to describe the flow behavior of these materials during consolidation.

As a consequence, squeeze flow may be a good choice for such a continuous measurement. It corresponds to the radial flow of a specimen subjected to axial compression [32]. Considering a Newtonian fluid, the most common squeeze flow model for polymers is Stefan's law which relates the applied force to the sample's thickness knowing the Newtonian viscosity and the squeeze rate [33]. Scott [34] has proposed an extension for power-law fluids which can be of particular interest for CF/PAEK composites [24,25,28,29]. However, both models assume isotropic flow, which is, as discussed previously, *a priori* inconsistent for CF/PEKK. Considering that the flow is only perpendicular to the fiber direction, Rogers [35] developed analytical relations for Newtonian fluids and square-shape samples. Only a few authors have proposed to measure the viscosity of composites by conducting squeeze flow experiments [36,37]. Thattaiparthasarthy et *al.* [36] were able to identify a power-law viscosity for long (but not continuous) glass fiber/-polypropylene by considering a transversely isotropic flow. Balasubramanyam et *al.* [37] tried to obtain a Newtonian viscosity of fiber reinforced thermoplastic composites (which nature is not precised) assuming an anisotropic flow with no-slip boundary conditions. The shear thinning behavior has been incorporated in an analytical model for anisotropic flows by Advani et al. [26] but according to the authors' knowledge, this modified Stefan's law has not been used to measure viscosities of continuous carbon fiber thermoplastic composites.

In this study, we aim at developing analytical models both for square and circular specimens, considering the anisotropic flow and shear-thinning rheological behavior. Squeeze flow experiments with varying parameters such as applied pressure, size and shape of the plates are then conducted to discuss the consistency of the models. The obtained composite viscosity results are finally compared to those obtained from oscillatory measurements using the experimental method proposed recently by Deignan et al. [24].

2. Materials and methods

2.1. Materials

The tapes used in the study were kindly provided by Hexcel. Continuous Hexcel High strength carbon fibers (Young's modulus $E \approx$ 240 GPa, tensile strength $\approx$ 5 GPa, diameter $\approx$ 7 μm [38]) are impregnated by PEKK matrix from Arkema ($E \approx$ 3.8 GPa, glass transition

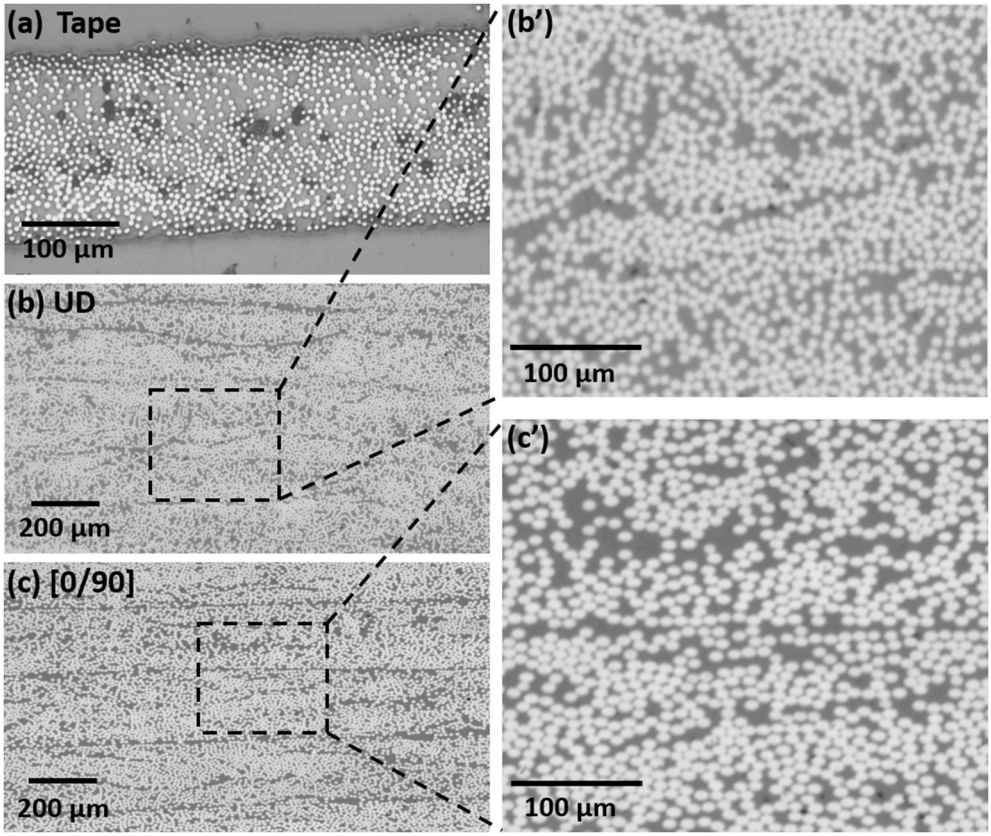

Fig. 1. Microstructure of (a) a CF/PEKK tape, (b) and (b') UD $[0]_8$ (b), and (c) and (c') $[0/90]_4$ laminates, as obtained by optical microscope (x200). The fibers are oriented perpendicular to the image (white circles). PEKK appears in light grey and porosities in dark grey/black. Note that for the cross-ply composites cut were made at 45° so that that fibers oriented at 0° or 90° appear at ±45° in the field of view (an image of a sample cut at 0° is shown in Fig. S1).

temperature $T_g = 162$ °C and melting temperature $T_m = 332$ °C [39]). The unidirectional (UD) tapes have a thickness close to 200 μm and an initial fiber volume and void content close to 55 %v and 5 %v respectively. A typical image of a CF/PEKK ply is given in Fig. 1a.

2.2. Laminates preparation

CF/PEKK laminates of 8 UD plies $[0]_8$ and 8 cross-plies $[0/90]_4$ having a surface of 150 mm × 150 mm have been consolidated in VBO prior to the squeeze flow experiments. The consolidated composites are considered void-free (i.e. for all samples, the void content is below 0.1%, as measured by optical microscopy in Fig. 1b and c). This protocol was applied to avoid inter-ply slip or additional gap decrease due to pore filling.

From the 150 × 150 mm consolidated samples, 25 mm diameter cylinders, 21 × 21 mm and 15 × 15 mm squares were cut by water jet. The samples were then dried 7 days in a vacuum oven at 130 °C prior any further experiment.

2.3. Apparatus and experimental methods

The squeeze flow experiments consist in compressing a composite sample at high temperature and studying the variation of the half-gap h, as a function of time (Fig. 2a). They are conducted on a DHR 20 rheometer from TA instrument using stainless steel square (21 mm or 15 mm) or circular geometries (25 mm diameter), as shown in Fig. 2b. The squeeze flow cycle used in these experiments is given in Fig. 2c. The samples are placed in the rheometer equipped with the chosen plates at 250 °C. A normal force of 1 N is applied in order to maintain a contact between the sample and the plates. A temperature ramp of 5 °C/min is applied up to 380 °C (the commonly used consolidation temperature for these matrixes [32]) under a force of 1 N. The sample is then let to rest at 380 °C and $F = 1$ N during 5 min to homogenize its temperature. Then, a given force is applied (for example, 45 N corresponds to ≈ 1 bar for 21 mm squares) and maintained at 380 °C for 30 min. The force ramp lasting about 1 s, much smaller than the experimental time, it will be neglected in the analysis. The initial half-thickness of the sample h_0 is taken at point A in Fig. 2c, *i.e.* at the moment where the force reaches its final value. The gap variation (*i.e.* the sample thickness) is recorded as a function of time. For each given condition, the experiments are conducted at least three times.

3. Analytical solutions for squeeze flow of power-law fluids

For square geometries, *i.e.* the configuration given in Fig. 2a, Advani et al. [26] already developed the analytical relationships to model the experimental squeeze flow behavior of continuous reinforced polymer composites by considering a power-law fluid (Eq. (1)). Briefly, we recall that similarly to Stefan's law, the model assumes the matter to be incompressible, neglects gravity and inertial terms. Moreover, the squeeze flow is considered to be slow and exclusively in the direction transverse to the fibers (only along x direction in Fig. 2a) with the lateral dimensions of the sample much higher than its thickness (*i.e.* $w, L \gg h$) leading to a flow velocity along x much higher than the one along z.

To confirm this hypothesis, the microstructure of a sample squeezed at constant force after 1 h of consolidation is studied (note that for this specific experiment, polyimide films were placed between the sample and the plate). From the rectangular shape obtained after compressing an initially square-shape UD CF/PEKK composite (white square in Fig. 3a), it is clear the major flow is perpendicular to the fiber direction. To be more precise, Fig. 3b and c shows the microstructure of the sample edges, along and transverse to the fibers' direction respectively. It can be seen that there is a small Darcy flow of matrix along the fibers (Fig. 3b). However, the contribution of Darcy flow volume is less than 5% of the flow volume in the transverse direction. Hence, as a first approach, its contribution will be neglected in the analytical model proposed and only the component 23 of the shear viscosity will be considered. Note this anisotropic flow is also observed on squeezed circular samples (see Fig. S2).

Based on the continuity and motion equations and considering a no-slip condition between the sample and the rheometer plates, one can derive the expression of pressure p along x (Eq. (2)). By integrating p on the rectangular surface $2wL$ (Fig. 2a), the expression of the force F can be obtained (Eq. (3)).

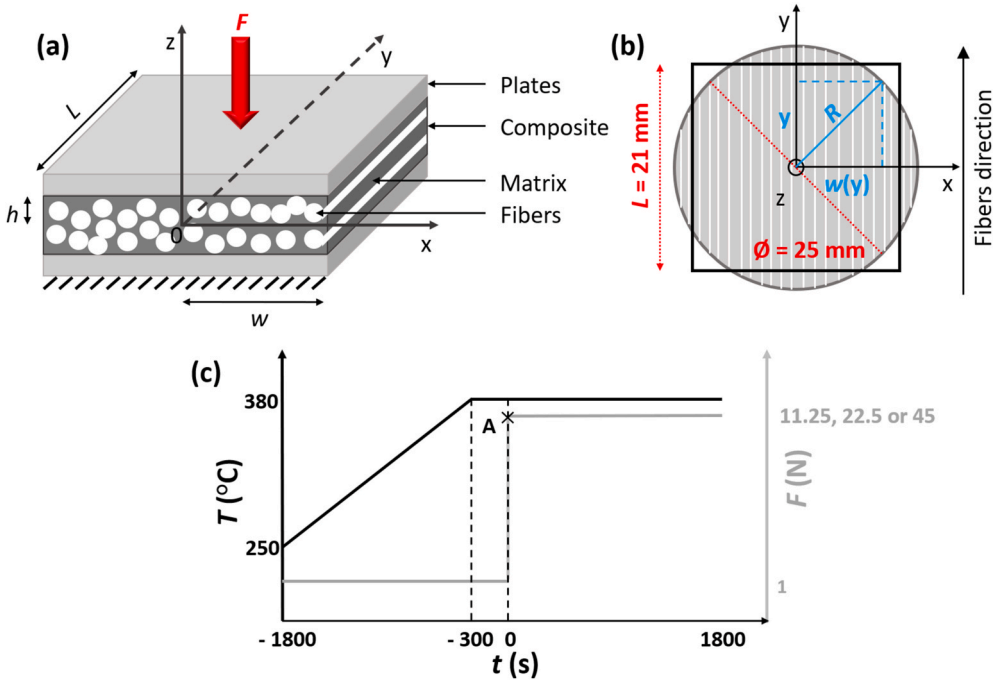

Fig. 2. (a) Squeeze flow experimental configuration on a rectangular geometry with 3D view and (b) corresponding top view for rectangular as well as circular geometries (c) Temperature and force (i.e. pressure) cycle applied during the squeeze flow experiment.

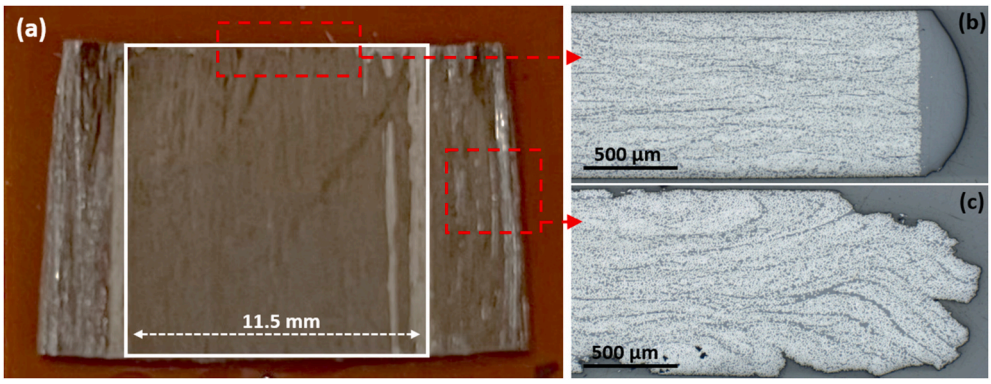

Fig. 3. (a) Picture of an initially square UD CF/PEKK sample (in white) after consolidation at 380 °C under 21 mm square plates at 22.5 N for 1 h. Optical microscopy image (x100) of the microstructure in the red area region (b) in the direction longitudinal and (c) transverse to the fibers, cut at 45°. (For interpretation of the references to colour in this figure legend, the reader is referred to the Web version of this article.)

$$p(x) = \frac{(-\dot{h})^n}{h^{1+2n}} \frac{K}{n+1}\left(\frac{2n+1}{n}\right)^n w^{n+1}\left(1-\left(\frac{x}{w}\right)^{n+1}\right) \tag{2}$$

$$F = \frac{(-\dot{h})^n}{h^{2n+1}}\left(\frac{2n+1}{n}\right)^n \frac{2K}{n+2} L w^{n+2} \tag{3}$$

where h is the half-thickness of the sample (Fig. 2a), $\dot{h}$ the squeeze rate, L and w respectively the length and the half-width of the sample.

The relation between the half-thickness of the sample and the experimental time is obtained by integrating Eq. (3) on a square surface of side $L = 2w$ and is given in Eq. (4):

$$\frac{1}{h^{1+\frac{1}{n}}} - \frac{1}{h_0^{1+\frac{1}{n}}} = \frac{n+1}{2n+1}\left(\frac{(n+2)F_0}{4\,K\,w^{n+3}}\right)^{\frac{1}{n}} t \tag{4}$$

where h_0 is the initial half-gap (or initial half-thickness) of the sample, F_0 the constant applied force and t the time.

As most of the rheometers are equipped with circular plates, it is of interest to develop equivalent relationships for circular geometries. It might also make the experiments easier as a precise angle alignment between the geometries and the sample is difficult for square geometries.

To switch from square configuration to circular one, let us consider the geometry change presented in Fig. 2b. As the flow only occurs in the transverse direction of the fibers (*i.e.* only in x direction), the initial circular shape of the geometry becomes progressively an ellipsoid in the x direction. The analytical relationships for circular geometries are based on the same hypotheses and boundary conditions as the square ones and are derived from Eq. (3) considering the geometry switch presented in Fig. 2b. Then, one can derive the expression of the infinitesimal force dF along y:

$$dF(y) = \left[\frac{2K}{n+2}\left(\frac{2n+1}{n}\right)^n \frac{(-\dot{h})^n}{h^{1+2n}}\right] w(y)^{n+2} dy \tag{5}$$

where $w(y)$ is the projection along x of the circular geometry edge, dependent on the position y (Fig. 2b). Expressing $w(y)$ as a function of R and y and by symmetry, the force F can be derived (Eq. (6)):

$$F = 2\left[\frac{2K}{n+2}\left(\frac{2n+1}{n}\right)^n \frac{(-\dot{h})^n}{h^{1+2n}}\right] \int_0^R \left(\sqrt{R^2-y^2}\right)^{n+2} dy \tag{6}$$

At a constant force $F = F_0$, the expression of the sample half-thickness as a function of time, for circular geometry, can be derived by integrating Eq. (6):

$$\frac{1}{h^{1+\frac{1}{n}}} - \frac{1}{h_0^{1+\frac{1}{n}}} = \frac{n+1}{2n+1}\left(\frac{(n+2)\,F_0}{4KR^{n+3}\int_0^1 (1-u^2)^{\frac{n}{2}+1} du}\right)^{\frac{1}{n}} t \tag{7}$$

Let us call I the following integral $I = \int_0^1 (1-u^2)^{\frac{n}{2}+1} du$. The values taken for I have been found to vary between 0.67 and 0.58 for n between 0 and 1 (Fig. S3). Its value will then be chosen constant in the following. As n is usually small for such materials (*i.e.* typically below 0.1 [21,22,29,32]), the value of I is set at 0.66.

We now compare this model developed for UD composites to experimental data on UD but also cross-ply stackings. Concerning the cross-ply laminates, the purpose is to verify the ability of the proposed model to describe the squeeze flow behavior of such stackings. Fig. 4 shows typical experimental squeeze flow data of UD and cross-ply CF/PEKK composites over 1800 s as well as the corresponding fit (obtained as in all the following using OriginPro® 2021) from Eq. (4). The modeling starts at point A (Fig. 2c). To better compare the differences between the geometries, the variation of the half-gap h is always normalized with the initial half-gap h_0 (at point A, Fig. 2c) and this ratio plotted as a function of time. A rapid decrease of the experimental curves followed by a progressive flattening can be noticed. The fitting of the cross-ply specimens seems to deviate from the experimental data much sooner (around 50 s) than the one of the UD composites (400 s). This is most certainly due to the fact that the effect of fiber locking prevents

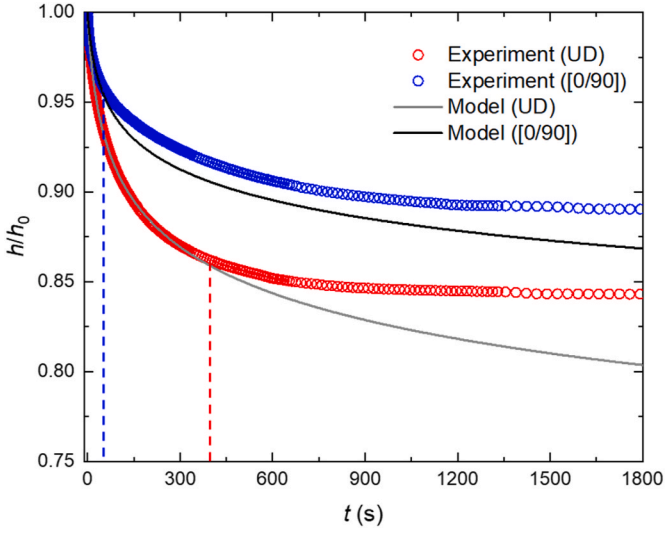

Fig. 4. Gap variation as a function of time of UD $[0]_8$ (red dots) and $[0/90]_4$ (blue dots) 21 mm square samples squeezed for 30 min at 380 °C and 45 N ($p \approx 1$ bar), with the associated fits on the whole experimental duration. The blue dotted line at 50 s and the red dotted one at 400 s mark the times at which the model deviates significantly from the experiment. (For interpretation of the references to colour in this figure legend, the reader is referred to the Web version of this article.)

further squeeze due to fiber-fiber contact at the ply-ply interface [40, 41], which is more pronounced and happens much faster for cross-ply composites than for UD ones. If we consider for example as a simple qualitative argument a volume fraction of 58% and a squared fiber organization [42], the mean fiber-to-fiber distance is 8.15 μm (for a fiber diameter of 7 μm). Assuming a total drying of the matrix (which is not the type of flow occurring here, as discussed previously), the relative maximum gap decrease is about 15 %. Though no direct comparisons should be made with the values obtained for the plateau observed in Fig. 4, fiber-fiber contact is a reasonable hypothesis to account for this experimental result. This effect not being considered in the model, discrepancies will occur at some point in time as the squeeze-flow modeling of h/h_0 will always tend to 0 for long experiments.

Hence, in further analysis, to gain precision we will focus on modeling the earlier stages of the squeeze flow experiments which are not impacted by fiber locking. At short times (typically <1 min), a cross-ply laminate has a squeeze flow similar to the one of a UD composite and can be seen as a superposition of individual UD plies. More precisely the model will be exploited during the first 400 s for all the conducted experiments on UD stackings and during the first 50 s for the cross-ply stackings. Though these values have been chosen somewhat arbitrarily (Fig. 4), it has been verified that the viscosity values extracted from the model do not differ significantly when this time window is changed. For example, when the considered time range is changed from 200 s to 500 s for UD samples, the variations on K and n obtained from the fits are less than 0.2 and 2 % respectively.

4. Results and discussion

4.1. Squeeze flow modelling of UD $[0]_8$ and $[0/90]_4$ CF/PEKK composites for square and circular geometries

In the time limit discussed previously, the gap variation as a function of time for UD composites along with the prediction from the model are given in Fig. 5a for square geometries and in Fig. 5b for circular ones. The shapes of the two curves are similar. The circular samples seem to squeeze less than the square ones, which can be explained by a slightly higher pressure applied on the square geometries (1 bar vs 0.9 bar). From the model, the viscosity parameters $K = 15{,}300$ Pa.s^n and $n = 0.04$ can be extracted for the square samples, and $K = 14{,}400$ Pa.s^n and $n = 0.02$ for the circular ones. As expected, the values from square and circular geometries are very similar.

The squeeze flow behavior of cross-ply $[0/90]_4$ composites have also been modeled during the first 50 s. The results are given in Fig. 5c for square geometries and Fig. 5d for circular ones. K and n values obtained for both geometries are again close to each other, and almost identical to the values obtained for UD samples. This confirms the validity of the model, and also indicates that UD and cross-ply composites flow similarly at short times, before fiber locking starts to play a major role in the squeeze flow response.

4.2. Effect of pressure and plate size

In the following, the applied force and the size of the samples (hence the corresponding pressure) are varied for square samples. Fig. 6a; b; c show the results for 15 mm square UD samples squeezed at 45 N ($p = 2$ bar), 22.5 N ($p = 1$ bar) and 11.25 N ($p = 0.5$ bar) respectively.

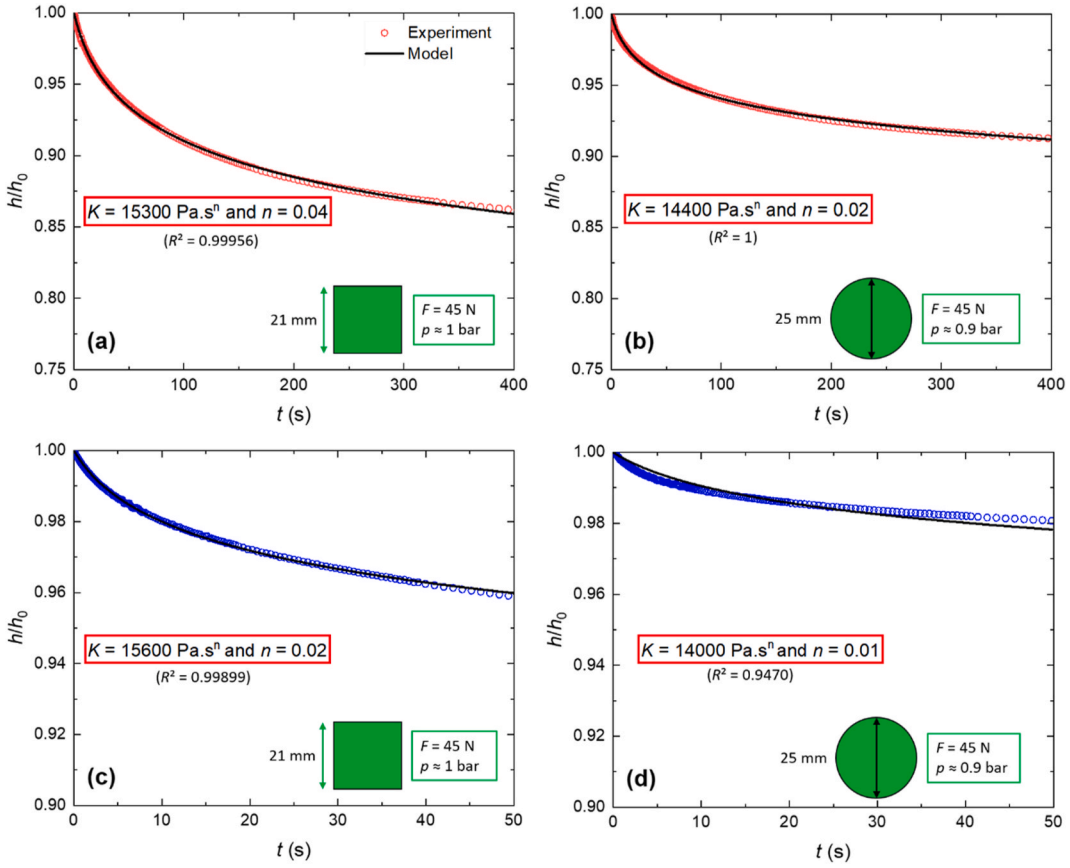

Fig. 5. Squeeze flow experimental data (circles) for UD $[0]_8$ (red, (a) and (b)) and $[0/90]_4$ samples (blue (c) and (d)), with the corresponding fits obtained from the model (lines) at 380 °C and 45 N, for (a)–(c) square geometries and (b)–(d) circular ones. (For interpretation of the references to colour in this figure legend, the reader is referred to the Web version of this article.)

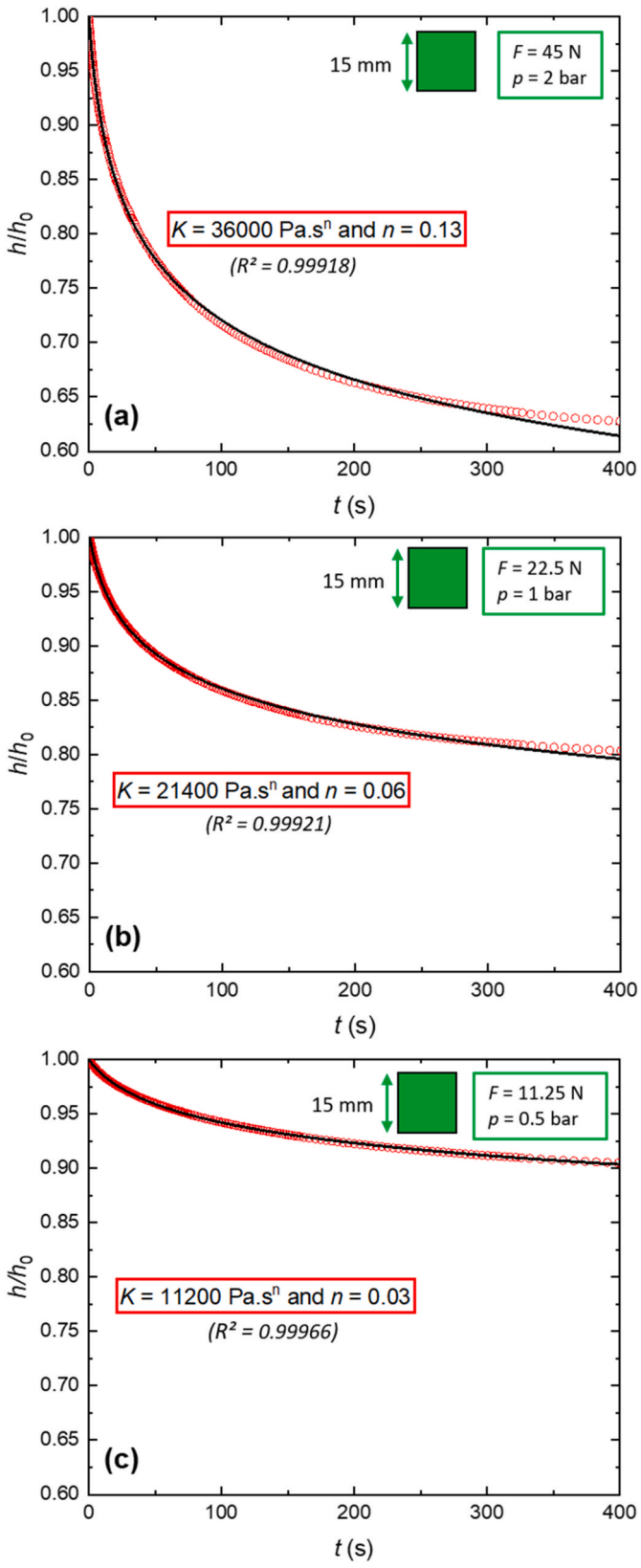

Fig. 6. Squeeze flow experimental data and corresponding fits of 15 mm square UD samples at 380 °C and (a) p = 2 bar; (b) p = 1 bar and (c) p = 0.5 bar.

The shape of the curves is again similar to the ones obtained in Fig. 5. For samples squeezed at higher pressure (Fig. 6a and b), the model deviates from the experimental curve sooner than for the low-pressure ones (Fig. 6c). This goes along with a more pronounced and faster decrease of the gap which can be related as before to fiber locking leading to discrepancies between the model and the experimental data.

The mean values for K and n are finally gathered, for all configurations, in Table 1.

The viscosity parameters also depend on the pressure applied: K and n both appear to increase linearly with the applied pressure in the range of the studied pressures (Fig. 7a and b). Fig. 7c shows the identified power-law curves obtained from the previous experiments on the UD square squeezed samples. For all cases, the power-law exponent is close to −1 and K is on the same range though values of K will differ with pressure, from 10,000 to 35,000 Pa.s^n with pressures ranging from 0.5 to 2 bar.

Focusing then on the size variation at a constant pressure, the squeeze flow behavior of 21 mm and 15 mm square samples can be compared at 1 bar (Figs. 5c and 6a). Though the gap reduction over time is similar, the viscosity parameters extracted from the model are different, especially again K (14,500 and 20,800 Pa.s^n).

However, if a power-law describes correctly the viscosity behavior of the composites, K and n vary with pressure or sample size. To try to understand these unexpected dependences, let us focus on the identified shear rate profile in the squeezed sample $\dot{\gamma}$ (x, z) (Eq. (8)).

$$\dot{\gamma}(x,z) = x\left(\frac{2^{n+1}(n+2)F}{KL^{n+3}}z\right)^{\frac{1}{n}} \tag{8}$$

As an example, the shear rate 3D-profile of the upper right part of the sample is given for F = 45 N and L = 21 mm (Fig. 8a and b). Due to symmetry along the x and z axes, the results can be duplicated in all parts of the sample. A similar profile of the shear rate has been observed for all conditions: almost no shear rate in most parts of the sample, with a sharp increase at the edges, and a maximum at the corners. At a given position in the thickness of the sample, the shear rate increases linearly with x. However, the increase of $\dot{\gamma}$ as a function of the height for a given x highly depends on n, hence on the applied pressure. To illustrate that, Fig. 8c shows how $\dot{\gamma}$ increases within the thickness of the sample for x at the edge (x = L) for different pressures.

In the light of this analysis, it can be noted that the differences obtained for K and n as a function of pressure and sample size are indeed significant. If we consider the 21 mm square samples squeezed at 1 bar with K and n values identical as those obtained at 1 bar for 15 mm squares, the applied force should be three times higher than the one applied on the 15 mm square to fit the gap evolution, which is not the case (it is only twice higher). At the same time, the maximum shear rate would be different by two orders of magnitude, which is not realistic.

Table 1
Viscosity parameters (K and n) averaged on 3 experiments for each configuration. The measurements uncertainty is given by the 95% confidence interval.

Stacking	Geometry	F (N)	Size (mm)	p (bar)	K (Pa.s^n)	n
$[0]_8$	circular	45	25	0.9	13,700 ± 1400	0.030 ± 0.014
$[0]_8$	square	45	21	1	14,500 ± 1000	0.047 ± 0.012
$[0]_8$	square	45	15	2	34,700 ± 1800	0.088 ± 0.047
$[0]_8$	square	22.5	15	1	20,800 ± 1100	0.055 ± 0.005
$[0]_8$	square	11.25	15	0.5	10,900 ± 400	0.031 ± 0.002
$[0/90]_4$	circular	45	25	0.9	14,100 ± 200	<0.01
$[0/90]_4$	square	45	21	1	15,600 ± 200	0.022 ± 0.003

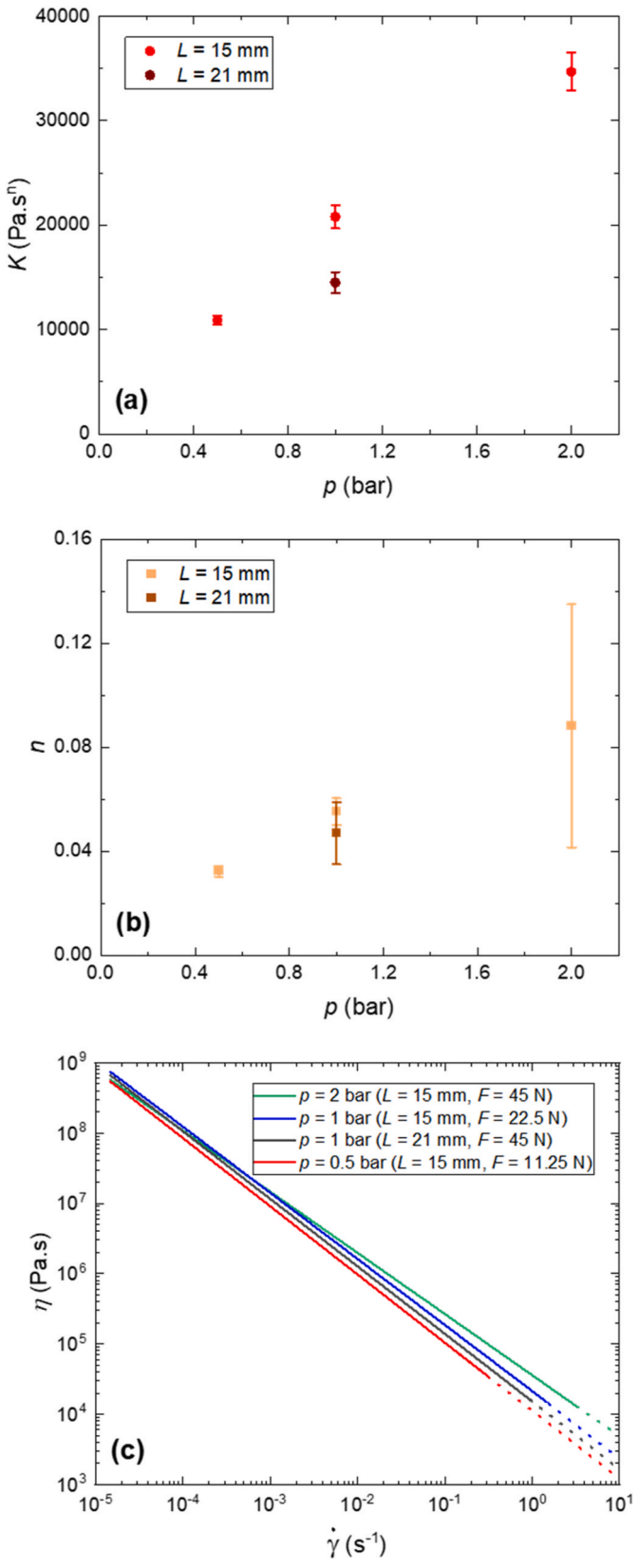

Fig. 7. Evolution of (a) K and (b) n as a function of the pressure p for square UD samples (L = 15 mm and L = 21 mm). (c) Reconstructed power-law viscosity profiles using K and n values obtained from the models for square UD samples.

Hence, we can hypothesize that the composite behaves like a yield-stress fluid, with a variation of K and n with pressure and size. Higher pressure or smaller plate size will induce higher shear rates and as a consequence a significant flow in a larger portion of the sample. This phenomenon (similar to shear-banding) was already observed by Deignan et al. [24] and is discussed in more details in the next section.

Nevertheless, squeeze flow experiments allow to obtain consistent values for K and n, and the variation of these parameters with pressure and size sample. This can be of interest to understand ~~and optimize~~ the consolidation processes of these composites (*i.e.* filling of voids) where pressure is one of the key parameters, especially for out-of-autoclave (low pressure) ones. As an example, an illustration of void filling is shown in Fig. S4.

4.3. Comparison with dynamic measurements

The previous sections showed that it was possible to extract viscosity profiles of CF/PEKK composites from squeeze flow experiments. This section aims at comparing these results to those obtained with an oscillatory measurement of CF/PEKK viscosity similar to the one proposed recently by Deignan et al. [24]. Keeping the methodology developed in this study, two off-centered consolidated UD 8 ply $[0]_8$ CF/PEKK samples with a length of 7.5 mm and a width of 2.5 mm are aligned at 5 mm from the center of the 25 mm circular geometry. Despite the low imposed strain, it has been verified for all experiments that the torque value is always significantly higher than the rheometer sensitivity. As in Ref. [24], the second moment of area in the transverse direction I_T is then much higher than the one in the longitudinal direction I_L, hence the storage and loss moduli in the transverse direction, respectively G'_T and G''_T, are expressed as follows:

$$G'_T = \left(\frac{2hM}{I_T\theta}\right)cos(\delta) G''_T = \left(\frac{2hM}{I_T\theta}\right)sin(\delta) \quad (9)$$

with M the amplitude of the torque, Θ the amplitude of the twist angle and δ the phase angle.

The test is conducted at a strain amplitude of 0.1%. It has been verified that this is in the linear viscoelasticity regime (see Fig. S5). The complex viscosities obtained for UD composites are given in Fig. 9 as a function of the angular frequency, at 3.1 bar and 0.5 bar (which are the pressures used in Ref. [24]). The viscosity profiles obtained at 0.5 and 2 bar (which is the maximum pressure that can be applied with our squeeze flow experiments) on 15 mm squares (Fig. 6a and c) are also displayed in Fig. 9 using the Cox-Merz rule.

First, it can be seen that dynamic measurements give complex viscosities that are much higher than viscosities from squeeze flow measurements. Note that the values obtained are also much higher than those obtained by Deignan on CF/PEEK at the same temperature [24]. This might be explained by the fact that their experiments were conducted at 5% of strain amplitude. Nonetheless, as in Ref. [24] for CF/PEEK, the complex viscosity of CF/PEKK obtained via the same method is highly dependent on the pressure applied: at 3 bar, the viscosity is three times higher than at 0.5 bar, because of a larger part of the composite that is deformed. This has been linked to shear-banding by the authors. As discussed previously, a similar effect is observed on our own measurements and is shown in Fig. 9.

Nevertheless, the values of complex viscosities obtained from dynamic measurements differ from almost 2 orders of magnitude with those obtained through continuous squeeze flow experiments. Simple squeeze flow experiments can then be used to obtain shear viscosity of continuous CF/PAEK composites, which will characterize the shear flow of the composite, for example during the consolidation process. With dynamic measurements no macroscopic flow occurs, and oscillatory shear will yield information on the composite relaxation times. It is clearly seen in Fig. 9 that both measurements are not equivalent for such highly filled composites, i.e. the Cox-Merz rule cannot be applied as

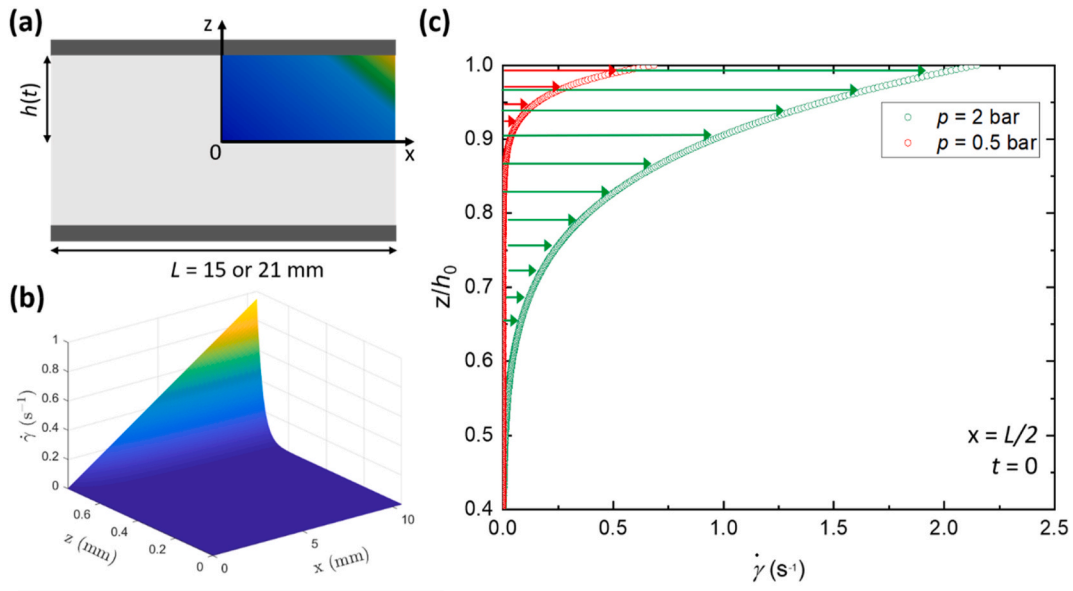

Fig. 8. (a) Schematic of the shear rate profile in the region of the squeezed square sample as described in (b). (b) Shear rate profile during the squeeze flow at 1 bar and any given y position (c) shear rate values along the z axis at t = 0, any y position and x = L/2 for 15 mm square samples squeezed at 0.5 and 2 bar.

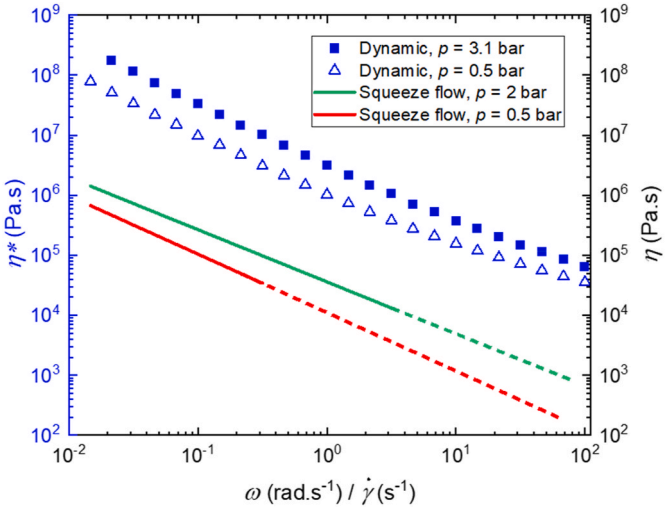

Fig. 9. Comparison between CF/PEKK viscosity profiles obtained through dynamic and squeeze flow measurements, at 380 °C under N_2.

already suggested in previous studies [29,30]. A more direct comparison could be between squeeze flow measurements and dynamic tests in the non-linear regime [29].

5. Conclusion

Monitoring the rheological behavior of CF/high performance thermoplastic composite such as CF/PEKK is essential to optimize the process with respect to the consolidation quality of the parts. It provides information on how easily the {fiber + matrix} system flows i.e. how the voids present within the plies can be filled.

In this study we showed that simple squeeze flow experiments coupled with analytical models considering the anisotropy of the flow and the geometry of the samples is a viable method to measure the viscosity parameters of the composite, assuming a power-law fluid behavior. We were able to describe quantitatively the squeeze flow at short times (i.e. before fiber locking) for both square and circular shaped specimens, for unidirectional and cross-ply stackings. Values on the order of 15,000 Pa.s^n and 0.02 are obtained for K and n respectively at 380 °C and pressures close to 1 bar, conditions similar to the ones encountered in out-of-autoclave processes.

An unexpected influence of the pressure and the size of the sample on K and n parameters was also observed. This can be explained by a flow with a strong heterogeneity of shear rate, and hence of stress in the flow, with shear mostly localized at the edges and maximum at the wall. The flow behavior is then similar to a yield-stress fluid for which an increase of applied pressure or a reduction in the size of the sample induces a greater portion of the fluid to flow, similar to shear-banding. We also show large discrepancies between these measurements and complex viscosities obtained through classical dynamic methods showing that the Cox-Merz rule cannot be applied for such systems.

The present work can help to understand the composite behavior in VBO, but we should state that these results cannot be directly extrapolated because the boundary conditions are not the same (constant force versus constant pressure). Nonetheless, from the squeeze flow results, we can understand that flow occurs at the edges of the plates while the shear rate will be very low in the center, meaning that the viscosity will be very high. This in turns leads to high consolidation times. The extracted viscosity parameters will allow to characterize the easiness of consolidation for a given composite.

Declaration of competing interest

The authors declare that they have no known competing financial interests or personal relationships that could have appeared to influence the work reported in this paper.

Data availability

Data will be made available on request.

Acknowledgments

This work was conducted under the framework of HAICoPAS, a PSPC project (projet de recherche et développement structurant pour la compétitivité) and of the Industrial Chair Arkema (Arkema/CNRS-ENSAM-Cnam). BPI France is acknowledged for funding the PhD work of R. Arquier (project number: PSPC.AAP-7.0_HAICoPAS). The authors thank Arkema, Hexcel, and more specifically N. Cadorin, M. Glotin, H.-

A. Cayzac, J. Pascal and Y. Deyrail for fruitful discussions.

Appendix A. Supplementary data

Supplementary data to this article can be found online at https://doi.org/10.1016/j.polymertesting.2023.108060.

References

[1] T.W. Clyne, D. Hull, An Introduction to Composite Materials. Second Edi, Cambridge Solid State Science Series, 2019.

[2] U.K. Vaidya, K.K. Chawla, Processing of fibre reinforced thermoplastic composites, Int. Mater. Rev. 53 (2008) 185–218, https://doi.org/10.1179/174328008X325223.

[3] T. Choupin, B. Fayolle, G. Régnier, C. Paris, J. Cinquin, B. Brulé, Isothermal crystallization kinetic modeling of poly(etherketoneketone) (PEKK) copolymer, Polymer 111 (2017) 73–82, https://doi.org/10.1016/j.polymer.2017.01.033.

[4] R. McCool, A. Murphy, R. Wilson, Z. Jiang, M. Price, J. Butterfield, et al., Thermoforming carbon fibre-reinforced thermoplastic composites, Proc. Inst. Mech. Eng. Part L J Mater Des Appl 226 (2012) 91–102, https://doi.org/10.1177/1464420712437318.

[5] G. Lesimple, I. Iliopoulos, J. Marijon, B. Fayolle, Full Characterization of Water Transport Properties in Polyetherketoneketone (PEKK), ACS Appl Polym Mater (2023), https://doi.org/10.1021/acsapm.2c01515 n.d.

[6] T. Choupin, L. Debertrand, B. Fayolle, G. Régnier, C. Paris, J. Cinquin, et al., Influence of thermal history on the mechanical properties of poly(ether ketone ketone) copolymers, Polym Cryst 2 (2019) 1–8, https://doi.org/10.1002/pcr2.10086.

[7] D. Veazey, T. Hsu, E.D. Gomez, Next generation high-performance carbon fiber thermoplastic composites based on polyaryletherketones, J. Appl. Polym. Sci. 134 (2017) 19–21, https://doi.org/10.1002/app.44441.

[8] H. Pérez-Martín, P. Mackenzie, A. Baidak, C.M. Ó Brádaigh, D. Ray, Crystallinity studies of PEKK and carbon fibre/PEKK composites: a review, Compos. B Eng. (2021) 223, https://doi.org/10.1016/j.compositesb.2021.109127.

[9] H. Pérez-Martín, P. Mackenzie, A. Baidak, C.M. Ó Brádaigh, D. Ray, Crystallisation behaviour and morphological studies of PEKK and carbon fibre/PEKK composites, Compos Part A Appl Sci Manuf 159 (2022), https://doi.org/10.1016/j.compositesa.2022.106992.

[10] F. Saffar, C. Sonnenfeld, P. Beauchêne, C.H. Park, In-situ monitoring of the out-of-autoclave consolidation of carbon/poly-ether-ketone-ketone prepreg laminate, Front Mater 7 (2020) 1–12, https://doi.org/10.3389/fmats.2020.00195.

[11] Y Di Boon, S.C. Joshi, S.K. Bhudolia, Review: filament winding and automated fiber placement with in situ consolidation for fiber reinforced thermoplastic polymer composites, Polymers 13 (2021) 1951, https://doi.org/10.3390/polym13121951.

[12] I. Martin, D. Saenz Del Castillo, A. Fernandez, A. Güemes, Advanced thermoplastic composite manufacturing by in-situ consolidation: a review, J Compos Sci 4 (2020) 1–36, https://doi.org/10.3390/jcs4040149.

[13] Z. Qureshi, T. Swait, R. Scaife, H.M. El-Dessouky, In situ consolidation of thermoplastic prepreg tape using automated tape placement technology: potential and possibilities, Compos. B Eng. 66 (2014) 255–267, https://doi.org/10.1016/j.compositesb.2014.05.025.

[14] R. Schledjewski, Thermoplastic tape placement process - in situ consolidation is reachable, Plast., Rubber Compos. 38 (2009) 379–386, https://doi.org/10.1179/146580109X12540995045804.

[15] M.J. Donough, St John NA. Shafaq, A.W. Philips, B. Gangadhara Prusty, Process modelling of In-situ consolidated thermoplastic composite by automated fibre placement – a review, Compos Part A Appl Sci Manuf 163 (2022), 107179, https://doi.org/10.1016/j.compositesa.2022.107179.

[16] N. Heathman, P. Koirala, T. Yap, A. Emami, M. Tehrani, In situ consolidation of carbon fiber PAEK via laser-assisted Automated fiber placement, Compos. B Eng. 249 (2022), 110405, https://doi.org/10.1016/j.compositesb.2022.110405.

[17] M. Coulson, L. Quiroga Cortés, E. Dantras, A. Lonjon, C. Lacabanne, Dynamic rheological behavior of poly(ether ketone ketone) from solid state to melt state, J. Appl. Polym. Sci. 135 (2018), https://doi.org/10.1002/app.46456.

[18] K. Ramaswamy, V. Modi, P.S. Rao, P.P. Martin, C.T. Mccarthy, R.M.O. Higgins, An investigation of the influence of matrix properties and fibre – matrix interface behaviour on the mechanical performance of carbon fibre-reinforced PEKK and PEEK composites, Compos Part A Appl Sci Manuf 165 (2023), 107359, https://doi.org/10.1016/j.compositesa.2022.107359.

[19] Z. Jin, Z. Han, C. Chang, S. Sun, H. Fu, Review of methods for enhancing interlaminar mechanical properties of fiber-reinforced thermoplastic composites: interfacial modification, nano-filling and forming technology, Compos. Sci. Technol. 228 (2022), 109660, https://doi.org/10.1016/j.compscitech.2022.109660.

[20] J.A. Goshawk, V.P. Navez, R.S. Jones, Squeezing flow of continuous fibre-reinforced composites, J Nonnewton Fluid Mech 73 (1997) 327–342, https://doi.org/10.1016/S0377-0257(97)00049-9.

[21] D.J. Groves, A.M. Bellamy, D.M. Stocks, Anisotropic rheology of continuous fibre thermoplastic composites, Composites 23 (1992) 75–80, https://doi.org/10.1016/0010-4361(92)90107-6.

[22] D.J. Groves, D.M. Stocks, Rheology of thermoplastic-carbon fibre composite in the elastic and viscoelastic states, Compos. Manuf. 2 (1991) 179–184, https://doi.org/10.1016/0956-7143(91)90137-6.

[23] T.G. Rogers, Rheological characterization of anisotropic materials, Composites 20 (1989) 21–27, https://doi.org/10.1016/0010-4361(89)90677-0.

[24] A. Deignan, W.F. Stanley, M.A. McCarthy, Insights into wide variations in carbon fibre/polyetheretherketone rheology data under automated tape placement processing conditions, J. Compos. Mater. 52 (2018) 2213–2228, https://doi.org/10.1177/0021998317740733.

[25] A. Deignan, Figiel, M.A. McCarthy, Insights into complex rheological behaviour of carbon fibre/PEEK from a novel numerical methodology incorporating fibre friction and melt viscosity, Compos. Struct. 189 (2018) 614–626, https://doi.org/10.1016/j.compstruct.2018.01.084.

[26] S.G. Advani, T.S. Creasy, S.F. Shuler, Chapter 8 Rheology of long fiber-reinforced composites in sheetforming, in: D. Bhattacharyya (Ed.), Compos. Sheet Form, Composite Materials Series, vol. 11, 1997, pp. 323–369, https://doi.org/10.1016/S0927-0108(97)80010-0. Elsiever.

[27] F.N. Cogswell, The processing science of thermoplastic structural composites, Int. Polym. Process. 1 (1987) 157–165, https://doi.org/10.3139/217.870157.

[28] W.F. Stanley, P.J. Mallon, Intraply shear characterisation of a fibre reinforced thermoplastic composite, Compos Part A Appl Sci Manuf 37 (2006) 939–948, https://doi.org/10.1016/j.compositesa.2005.03.017.

[29] S.P. Haanappel, R. Akkerman, Shear characterisation of uni-directional fibre reinforced thermoplastic melts by means of torsion, Compos Part A Appl Sci Manuf 56 (2014) 8–26, https://doi.org/10.1016/j.compositesa.2013.09.007.

[30] T. Kitano, T. Kataoka, Y. Nagatsuka, Dynamic flow properties of vinylon fibre and glass fiber reinforced polyethylene melts, Rheol. Acta 416 (1984) 408–416.

[31] T. Kaully, A. Siegmann, D. Shacham, Rheology of highly filled natural CaCO 3 composites . II . Effects of solid loading and particle size distribution on rotational rheometry, Polym. Compos. 28 (2007) 524–533, https://doi.org/10.1002/pc.

[32] R. Arquier, I. Iliopoulos, G. Régnier, G. Miquelard-Garnier, Consolidation of continuous-carbon-fiber-reinforced PAEK composites : a review, Mater. Today Commun. 32 (2022), https://doi.org/10.1016/j.mtcomm.2022.104036.

[33] J. Stefan, Versuche über die scheinbare Adhäsion, Ann Der Phys Und Chemie 230 (1875) 316–318, https://doi.org/10.1002/andp.18752300213.

[34] J.R. Scott, Theory and application of the parallel-plate plastimeter, Trans Inst Rubber Ind 7 (1931) 169–186.

[35] T.G. Rogers, Squeezing flow of fibre-reinforced viscous fluids, J. Eng. Math. 23 (1989) 81–89, https://doi.org/10.1007/BF00058434.

[36] K.B. Thattaiparthasarthy, S. Pillay, U.K. Vaidya, Rheological characterization of long fiber thermoplastics - effect of temperature, fiber length and weight fraction, Compos Part A Appl Sci Manuf 40 (2009) 1515–1523, https://doi.org/10.1016/j.compositesa.2009.06.009.

[37] R. Balasubramanyam, R.S. Jones, A.B. Wheeler, Modelling transverse flows of reinforced thermoplastic materials, Composites 20 (1989) 33–37, https://doi.org/10.1016/0010-4361(89)90679-4.

[38] Hexcel Corporations, HexTow ® AS7 carbon fiber, Tech Data Sheet (2020). https://www.hexcel.com/user_area/content_media/raw/AS7_Aerospace_HexTow_DataSheet.pdf.

[39] Kepstan Arkema, PEKK Resins for Thermoplastic Composites Tech DataSheet, 2018. https://mypolymer.materialdatacenter.com/pds/en/si/kepstan7002.

[40] J.A. Barnes, F.N. Cogswell, Transverse flow processes in continuous fibre-reinforced thermoplastic composites, Composites 20 (1989) 38–42, https://doi.org/10.1016/0010-4361(89)90680-0.

[41] G.B. McGuinness, C.M. Ó Brádaigh, Characterisation of thermoplastic composite melts in rhombus-shear: the picture-frame experiment, Compos Part A Appl Sci Manuf 29 (1998) 115–132, https://doi.org/10.1016/S1359-835X(97)00061-4.

[42] B. Thomas Astrom, R. Byron Pipes, S.G. Advani, On flow through aligned fiber beds and its application to composites processing, J. Compos. Mater. 26 (1992) 1351–1373.